![The University of Edinburgh logo]

Edinburgh Research Explorer

Single-Molecule Magnetism, Enhanced Magnetocaloric Effect, and Toroidal Magnetic Moments in a Family of Ln4 Squares

![OPEN ACCESS logo]

Single-Molecule Magnetism, Enhanced Magnetocaloric Effect and Toroidal Magnetic Moments in a Family of Ln4 Squares

Chinmoy Das,[a] Shefali Vaidya,[a] Tulika Gupta,[a] Jamie M. Frost,[c] Euan K Brechin,[c] Mattia Righi,[b] Marco Affronte*,[b] Gopalan Rajaraman*,[a] and Maheswaran Shanmugam*,[a]

Three cationic [Ln4] squares (Ln = lanthanide) have been isolated as single crystals and their structures solved as $[Dy_4(\mu_4\text{-}OH)(HL)(H_2L)_3(H_2O)_4]Cl_2\cdot(CH_3OH)_4\cdot(H_2O)_8$ (**1**), $[Tb_4(\mu_4\text{-}OH)(HL)(H_2L)_3(MeOH)_4]Cl_2\cdot(CH_3OH)_4\cdot(H_2O)_4$ (**2**) and $[Gd_4(\mu_4\text{-}OH)(HL)(H_2L)_3(H_2O)_2(MeOH)_2]Br_2\cdot(CH_3OH)_4\cdot(H_2O)_3$ (**3**). Their structures describe an hydroxo-centred square of lanthanide ions, with each edge of the square bridged by a doubly deprotonated H_2L^{2-} ligand. Alternating current (ac) magnetic susceptibility measurements show frequency dependent out-of-phase signals with two different thermally assisted relaxation processes for **1**, but no maxima in χ_M'' appears above 2.0 K for complex **2**. For **1**, the estimated effective energy barrier for these two relaxation processes is found to be 29 K and 100 K. Detailed *ab initio* studies reveal that complex **1** possesses a toroidal magnetic moment. *Ab initio* calculated anisotropies of complex **1** and **2** are employed to simulate the magnetic susceptibility using the Lines model (POLY_ANISO) and this procedure yields J_1 = +0.01 and J_2 = -0.01 cm^{-1} (for **1**); J_1 = +0.11 and J_2 = -0.01 cm^{-1} (for **2**) as the two distinct exchange interactions between the Dy(III) and Tb(III) ions. Similar parameters are also obtained for complex **1** and **2** from specific heat measurements. A very weak antiferromagnetic super exchange interaction (J_1 = -0.043 cm^{-1} and g = 1.99) is witnessed between the metal centres in **3**. The magnetocaloric effect (MCE) was estimated using field dependent magnetization and temperature dependent heat capacity measurements. An excellent agreement is found in the $-\Delta S_m$ values extracted from these two measurements for all three complexes. As expected, **3** shows the largest $-\Delta S_m$ variation (23 J Kg^{-1} K^{-1}) among the three complexes. The negligible magnetic anisotropy of Gd indeed ensures near degeneracy in the (2S +1) ground state microstates, and the weak super-exchange interaction facilitates dense population of low-lying excited states all of which are likely to contribute to the MCE, making complex **3** an attractive candidate for cryogenic refrigeration.

Introduction

The large magnetic moments and unquenched first order orbital angular momenta associated with certain lanthanide ions makes their coordination complexes potentially useful in various applications such as information storage,[1] spintronics,[2] molecular switches,[3] spin valves [4] and qubits[5]. The academic investigation of the magnetic behaviour of lanthanide-based molecular cages has been reinvigorated since the discovery of single-molecule-magnet (SMM) behaviour in a mononuclear terbium phthalocyanine complex.[6] Following this, several lanthanide based SMMs, in particular dysprosium based clusters ranging from monomers to tetracosanuclear species, have been reported.[1h, 7] Among them more often, multinuclear clusters show unusual magnetic properties, for fascinating recent examples include Dy3 triangles in which SMM

behaviour was observed to originate from the excited states,[8] Dy5 and Dy4K2 clusters exhibiting enormous U_{eff} values[1b], and the presence of magnetic bistability in symmetric oligomeric lanthanide complexes due to a toroidal arrangement of anisotropic axes.[7b] Although various promising synthetic approaches have been reported to increase the effective energy barrier to the reorientation of the magnetization of SMMs, the blocking temperature (T_B) associated with the onset of hysteresis in molecular systems still sits below T = 14 K,[9] hampering any realistic development of molecular devices for practical application. This is partly due to the lack of understanding of the combined roles of orbital (L) and spin (S) angular momenta to the resultant magnetic moment of the molecule. Moreover, further complication may arise due to the changing contribution of L and S with changing geometry around the lanthanide ions.[10] Molecular complexes constructed by metal ions

with negligible magnetic anisotropy such as Gd(III) have been proposed for various applications, including contrast agents in magnetic resonance imaging,[11] spin-labeling,[12] dynamic nuclear polarization,[13] and cryogenic refrigeration, which takes advantage of the materials intrinsic magnetocaloric effect (MCE).[14] Traditionally ^{3}He-^{4}He has been used to attain sub-milli Kelvin temperatures, but as well as being environmentally unfriendly; the transfer of cryogenic liquid ^{3}He-^{4}He requires a complicated mechanical set-up. Following the proposed idea of employing nanoparticles for magnetic refrigeration by Shull and co-workers,[15] a plethora of 0-3D molecule-based materials have been reported as promising candidates, particularly by Evangelisti and co-workers who recently pointed out the importance of a large magnetic density (*i.e.* the use of lightweight ligands) in achieving improved MCE efficiency, together with large S and weak J.[14e, 16]

In this line of interest and to reveal a new generation of lanthanide based clusters with both isotropic and anisotropic lanthanide metal ions we have employed an underemployed multidentate Schiff-base ligand (H$_4$L, Scheme 1), which has previously been used to make just seven transition metal complexes,[17] four 3d-4f metal complexes (four complexes),[18] and three 4f complexes.[19]
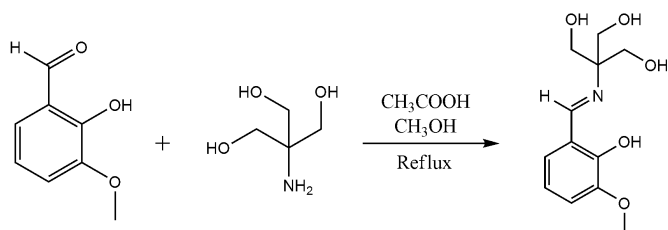
Scheme. 1 Synthetic scheme followed to make H$_4$L See the Experimental section for full details.

In this article, we report three analogous Ln$^{III}_4$ squares of general formula [Ln$_4$(μ_4-OH)(HL)(H$_2$L)$_3$(Y)$_4$]X$_2$ cluster (Ln = Dy(III), Tb(III), Gd(III); Y = solvent, X = halide) whose structures were determined by single crystal X-ray diffraction, whose magnetothermal properties have been gauged *via* variable temperature, variable field susceptibility, magnetization and specific heat measurements. To further support our experimental findings we have performed CASSCF+RASSI-SO calculations. This detailed experimental and theoretical investigation reveals that complex **1** exhibit a rare toroidal magnetic moment which is evident from the magnetization measurements (*vide infra*) and complex **3** shows large variation in -ΔS_m, making it a promising candidate for cryogenic refrigeration.

Results and Discussion

The reaction between the Schiff-base ligand H$_4$L and lanthanide halide (DyCl$_3$·6H$_2$O or TbCl$_3$·6H$_2$O or GdBr$_3$·6H$_2$O) in the presence of NaOMe in methanol results in the formation of pale yellow single crystals of complexes **1-3** after one week. X-ray diffraction reveals the structure to be [Ln$_4$(μ_4-OH)(HL)(H$_2$L)$_3$(Y)$_4$]X$_2$ (where Ln = Dy(III), Y = H$_2$O, X = Cl (**1**); Ln = Tb(III), Y = MeOH, X = Cl (**2**); and Ln = Gd(III), Y = MeOH, X = Br (**3**)). The molecular structures

of all the three (isomorphous) complexes are given in Figure 1, and their corresponding crystallographic data listed in Table 1.
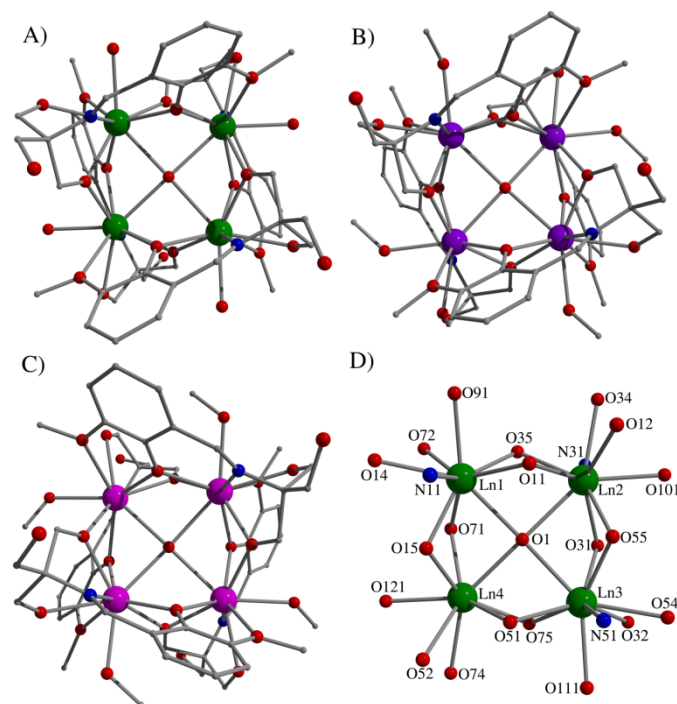
Fig 1. Ball and stick representation of single crystal X-ray structures of the cations of complexes **1** (A), **2** (B) and **3** (C). D) The general metal core found in **1-3**. The same labelling scheme has been followed for all the three complexes.

The lanthanide ions are in their usual trivalent oxidation state, and occupy the corners of a square, at the centre of which lies a μ_4-OH$^-$ ion, linking all the four lanthanide ions. The oxidation state of this μ_4-bridging O-atom was confirmed by bond valence sum calculation (Table S1).[20] The Ln ions in these complexes are however not co-planar, there being a small twist of 19° (for **1**) and 18.8° (for **2** and **3**) in the dihedral angle within the Ln$_4$ plane (Figure 2D). The μ_4-OH$^-$ ion possesses distorted square planar geometry in all the three complexes (Figure 2). The average diagonal bond angles found in these complexes are ∠Ln1O1Ln3 = 166.2° and ∠Ln2O1Ln4 = 166.6°.

The bond lengths between Ln(III) ions and the central hydroxide ion range from 2.506 Å to 2.529 Å (for **1**), 2.494 Å to 2.553 Å (for **2**) and from 2.506 Å to 2.586 Å (for **3**). The average Ln-Ln distance is found to be 3.577 Å (for **1**), 3.592 Å (for **2**) and 3.623 Å (for **3**). Each edge of the square is bridged by one phenoxo oxygen (from the *o*-vanillin moiety) from one H$_2$L^{2-} and an alkoxo group from hydroxymethyl arm of a second H$_2$L^{2-} ligand. The remaining coordination sites of the Ln ions are filled by methoxy oxygen atoms of *o*-vanillin, azomethine nitrogen atoms, the O-atom from the second arm of the hydromethyl group of H$_2$L^{2-} (the third arm of the latter remains protonated and non-bonded), and terminally bonded water and methanol molecules. There is a significant difference in the observed Ln-O bond lengths between the bridging alkoxide (2.262-2.320 Å (**1**), 2.278- 2.322 Å (**2**) and 2.297- 2.362 Å (**3**)) and

the terminally bonded alcohol (2.453-2.514 Å (**1**), 2.457-2.492 Å (**2**), and 2.479- 2.511 Å (**3**)), suggesting the latter to be protonated.

Table 1. Crystallographic parameters for the complexes **1-3**

	1	2	3
Formula	$C_{48}H_{68}N_4O_{25}Cl_2Dy_4$	$C_{52}H_{72}N_4O_{25}Cl_2Tb_4$	$C_{52}H_{72}N_4O_{25}Br_2Gd_4$
Size [mm]	0.17 x 0.12 x 0.09	0.16 x 0.11x 0.08	0.16 x 0.13 x 0.09
System	Triclinic	Triclinic	Triclinic
Space group	$P\text{-}1$	$P\text{-}1$	$P\text{-}1$
a [Å]	14.000(3)	13.914(5)	14.029(7)
b [Å]	15.650(3)	15.625(6)	15.692(8)
c [Å]	17.790(4)	18.201(7)	18.363(9)
α[°]	101.07(3)	102.620(4)	103.411(7)
β [°]	91.48(3)	92.951(5)	92.689(5)
γ[°]	106.25(3)	105.233(5)	105.499(7)
V [Å^3]	3659.3(13)	3701(2)	3764(3)
Z	2	2	2
ρ_{calcd}[g/cm^{-3}]	1.654	1.669	1.714
$2\Theta_{max}$	47.64	58.26	50.64
radiation	MoK$_\alpha$	MoK$_\alpha$	MoK$_\alpha$
λ [Å]	0.71073	0.71075	0.71073
T [K]	100	100	100
Reflns	27407	65208	50807
Ind. reflns	11213	19250	13500
reflns with $I>2\sigma(I)$	6798	15596	11560
$R1$	0.0660	0.0689	0.0806
$wR2$	0.1562	0.1825	0.2266

The charge balance requirements further support this assumption, two halide counter ions present in the crystal lattice neutralizes the cationic charge on the coordination sphere. The third arm of the hydromethyl group of H_2L^{2-} (which remains uncoordinated) facilitates the intermolecular hydrogen bonding (O13….O73 = 2.721 Å; O33…O53 = 2.611 Å; C12….O73 = 2.636 Å; C17….O73 = 2.657 Å).
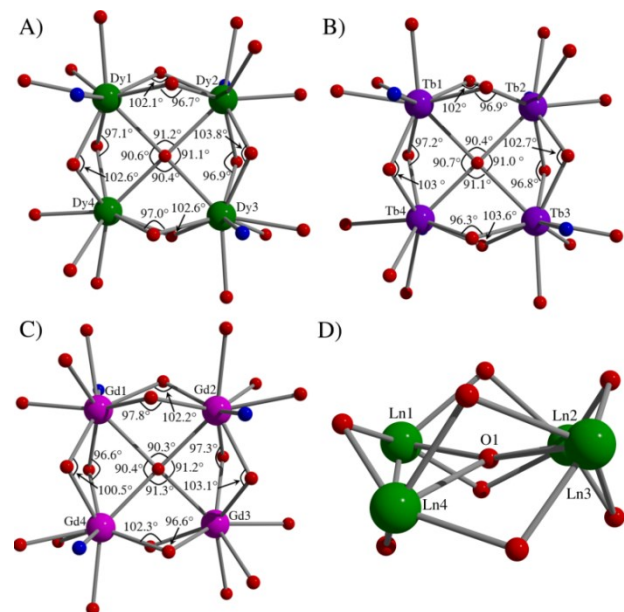

Fig 2. Average bond lengths and bond angles for **1-3** (A-C). D) A view showing the distortion observed in Ln4 square (The average dihedral angle is 19°).

By careful analysis of bond length of uncoordinated hydromethyl group of all the Schiff base ligands in **1** reveals that C19-O13 (1.332 Å) has significantly shorter bond length than the other three (C39-O33 (1.401 Å), C59-O53 (1.425 Å), and C79-O73 (1.410 Å)) unbound hydromethyl arms. This evidently suggests that among the four non-bonded hydromethyl arm of ligand, C19-O13 arm is deprotonated, thus balancing the trivalent cationic charge on the coordination sphere along with two halides in the crystal lattice. (See ESI Figure S1 for complete molecule labelling) A similar trend is also followed in case of structurally analogous **2** and **3**.

Each lanthanide ion (in **1-3**) is surrounded by nine donor atoms (LnO_8N_1) and exists in a distorted monocapped square anti-prismatic geometry, as confirmed by continuous SHAPE measurement software.[21] The square [Ln4-μ_4-OH] core is rather rare, limited to only three complexes, based on a search of the Cambridge Structural Database (CSD).[22] For example, Wong and co-workers reported the complex [Ln$_4$(μ_4-O)L$_2$(NO$_3$)$_4$(MeOH)$_2$] (Ln = Gd and Tb; L = 1,3-bis(2-hydroxy-3-methoxybenzylamino)propan-2-ol) in 2001, in which the Ln ions are eleven coordinate,[22c] and Thompson *et al* reported a series of [2 X 2] square grids of formula [Ln$_4$(L1)$_4$(μ_4–O)(μ_2–1,1–N$_3$)$_4$] (Ln = Dy and Tb) using carbohydrozone (L1) ligands.[22b,23] In the latter each metal ion is surrounded by nine donor atoms with capped square anti-prismatic geometry around the metal ions.

Magnetic susceptibility

Temperature dependent dc magnetic susceptibility measurements on polycrystalline samples of **1 - 3** were carried out between 300 and 2.0 K in an external magnetic field of $H = 0.1$ T (Figure 3). The observed room temperature $\chi_M T$ values of 55.60 (for **1**), 47.20 (for **2**) and 30.98 cm^3 K mol^{-1} (for **3**) are slightly lower than the expected values of 56.67 cm^3 K mol^{-1} ($g = 4/3$; S = 5/2; L =5; $^6H_{15/2}$ for **1**), 47.25 cm^3 K mol^{-1} ($g = 3/2$; $S = 3$; $L = 3$; $^7F_6$ for **2**) and 31.5 cm^3 K mol^{-1} ($g = 2.0$; $S = 7/2$; $L = 0$, $^8S_{7/2}$ for **3**) for a magnetically dilute Dy(III), Tb(III) and Gd(III) ions, respectively. The $\chi_M T$ values for **1** and **2** gradually decrease from room temperature to 45 K, likely due to the depopulation of e m_J levels, with the depopulation effect being more evident in **1** than **2**. The $\chi_M T$ value drops rapidly below 45 K, and reaches a value of 25.4 cm^3 K mol^{-1} (for **1**), 26.99 cm^3 K mol^{-1} (for **2**) at 5.0 and 2.5 K respectively. On the contrary, for **3**, the $\chi_M T$ value remains constant from room temperature to 100 K, below which it steadily decreases before rapidly reducing below 35 K to a value of 12.95 cm^3 K mol^{-1} at 2.31 K. The decrease in $\chi_M T$ value of all the three complexes at lower temperature is due to the combined effects of some or all of the following phenomena: magnetic anisotropy (**1**, **2**), intramolecular antiferromagnetic exchange interactions, Intermolecular dipolar exchange interactions, thermal depopulation effects.

Isothermal magnetization $M(H)$ measurements performed on polycrystalline samples of **1- 3** are summarized in Figure 3, with full details reported in the ESI (Figures S2-S4). From Figure 3 it is evident that complexes **1** and **2** show saturation at ~19.3 M/Nμ_B and ~15.3 $M/N\mu_B$ at 2.0 and 2.2 K, respectively – values which are approximately half the expected value for four very weakly coupled

lanthanide ions, indicating the presence of significant magnetic anisotropy,[1h] and consistent with the non-superimposable reduced magnetization curves (Figure S5). On the contrary the magnetization of complex **3** is as one might expect for four weakly coupled, isotropic Gd(III) ions, with M close to saturating at a value of $M/N\mu_B$ = 28.
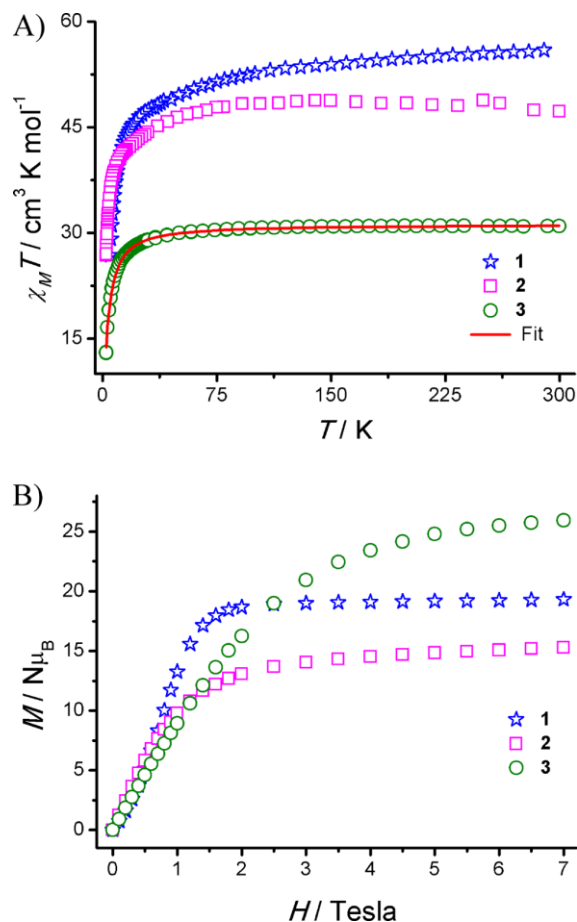

Fig 3. A) Variable-temperature dc $\chi_M T$ plot of polycrystalline samples of **1–3**, measured with an applied field of 0.1 T. The red line denotes the best fit obtained for the parameters given in the text; B) Isothermal field dependent magnetization measurement of **1-3** measured from 0-7 T at $T = 2.2$ K.

In order to extract the spin Hamiltonian parameters for the isotropic cluster **3**, magnetic susceptibility data were fitted by matrix diagonalization using Phi software.[24] Based on the crystal structure parameters of **3**, we initially employed two different J values: J_1 corresponding to nearest neighbour interactions round the 'outside' of the square where the super-exchange interaction is mediated between the metal ions *via* phenoxo, alkoxo and μ_4-hydroxide bridges, whereas J_2 relates to next nearest neighbour (diagonal) interactions (Gd1O1Gd3 and Gd2O1Gd4) mediated exclusively by the central μ_4-hydroxide. The Heisenberg Hamiltonian used for fitting the data is shown in the equation below. The experimental data were very well reproduced with the following parameters $J_1 = -0.043$ cm^{-1}, $J_2 = -0.043$ cm^{-1} with $g = 2.0$. Since $J_1 = J_2$ we repeated the fit with just one J value which afforded $J_1 = -0.043$ cm^{-1} and $g = 1.99$ (Figure 3). The fitting parameters clearly suggest that the exchange is very weak and the cluster can essentially be regarded as

a paramagnet. Such weak exchange interactions between the metal centres is an essential ingredient for observing an enhanced MCE (*vide infra*).

$$H = -2(J_1 S_{Gd1} \cdot S_{Gd2} + J_1 S_{Gd2} \cdot S_{Gd3} + J_1 S_{Gd3} \cdot S_{Gd4} + J_1 S_{Gd1} \cdot S_{Gd4}) - 2 (J_2 S_{Gd1} \cdot S_{Gd3} + J_2 S_{Gd2} \cdot S_{Gd4}) + m_s g \mu_B H$$

In order to probe the magnetization relaxation dynamics of both **1** and **2**, alternating current (ac) magnetic susceptibility measurements were performed on polycrystalline sample of **1** (Figure 4) and **2** (Figures S6-S7) at various frequencies.
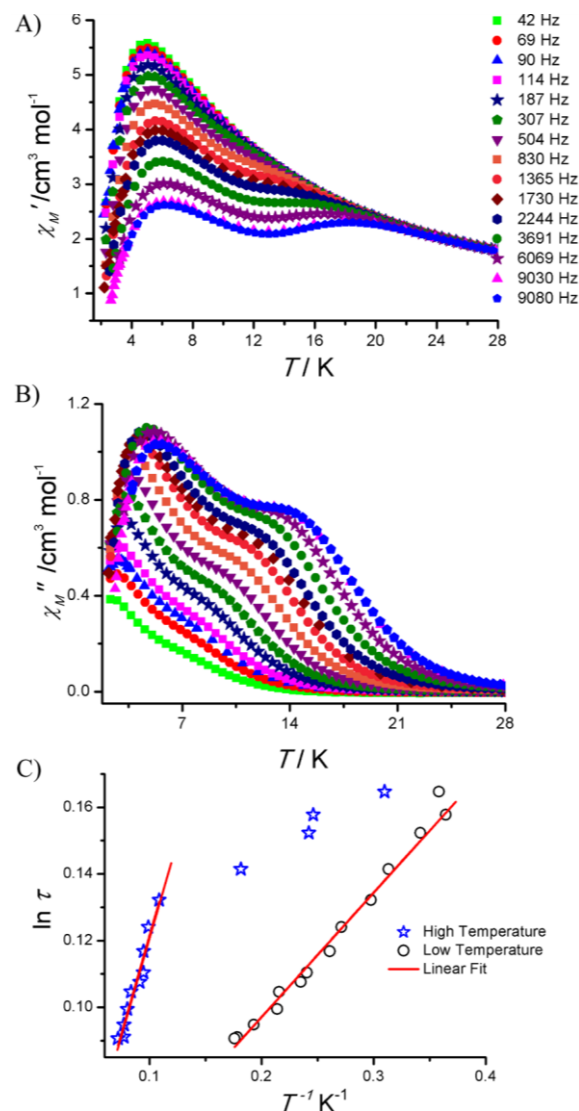

Fig 4. Frequency dependent A) in-phase, B) out-of-phase ac magnetic susceptibility (χ_M'') for **1** at the indicated frequencies. C) Arrhenius plot constructed for the both slow and fast relaxation processes.

For **2**, the maxima in χ_M'' is well below the instrument temperature limit under zero external magnetic field (Figure S7). On the contrary, for complex **1** there are two thermally assisted χ_M'' signals with maxima clearly evident corresponding to fast and slow magnetization relaxation processes at low ($T = 2.5$ - 5.2 K) and high ($T = 3.0$ - 15 K) temperatures, respectively (Figure 4). Similar

behaviour was recently reported in analogous tetrameric clusters by Layfield and co-workers.[25] However, the origin of two magnetization relaxations in this reported complex is distinctly different from **1** (*Vide infra*). Lanthanide complexes are prone to exhibit fast quantum tunneling of magnetization (QTM),[1b] likely to be operable in the low temperature region, however the thermally assisted Orbach process appears to be the dominant relaxation process in complex **1**. Observation of frequency dependent out-of-phase susceptibility (χ_M'') signals (for **1**) is a characteristic signature of SMM behaviour under zero applied external magnetic field. The Arrhenius plot constructed for these high and low *T* regimes are shown in Figure 4C. The effective energy barrier (U_{eff}) for the reorientation of magnetization for the fast and slow relaxation processes are 29 K and 100 K with $\tau_0 = 1.324 \times 10^{-7}$ s and $\tau_0 = 1.179 \times 10^{-8}$ s, respectively. The deviation from linearity for the slow relaxation process below 7.0 K suggests that other relaxation processes, such as Raman and Direct processes, are also likely to be operable.[10e,26]

Theoretical Studies

In order to understand the electronic structures of anisotropic metal complexes **1** and **2** detailed *ab initio* calculations were performed (see ESI for computational details and Figure S8). Two sets of calculations were performed on complex **1**. The first, using the SINGLE_ANISO program, calculated the magnetic anisotropy of the individual Dy(III) ions; the second, using the POLY_ANISO program, was employed to extract the exchange-coupled energy levels and the exchange parameters. We begin our discussion with the calculation of the single ion anisotropy parameters.

Single-ion anisotropy of Dy(III): The energy spectrum and *g*-tensors for the Kramers doublets of the ground $^6H_{15/2}$ multiplet for the four Dy(III) ions in compound **1** are shown in the ESI (Tables S2-S5), with the excited states lying at 3000 cm^{-1}. In **1**, the ground state (GS) Kramers Doublet (KD, Figure 5) shows an almost Ising type anisotropy for all four metal sites (Table 2) *i.e.* g_{zz} is close to 20, with a small transverse anisotropy in the y direction. The axiality of the *g*-tensors gradually decreases up to Kramers doublets 3 and 4 (Tables S2-S5), thereafter increasing reaching axiality for the eighth Kramers doublet which is comparable to the value of lowest Kramers Doublet (close to 20). The observation of such mirror symmetry in the magnetic properties in the Kramers doublets is in sharp contrast to the trend in perfectly axial systems. The relative energies of the eight lowest lying KDs along with the computed anisotropy for all four Dy(III) ions in complex **1** are given in Tables S2-S5. The ground state is found to possess zero magnetic moment in the xy plane and it is entirely oriented along the z-axis (L_z). The two lowest Kramers doublets, shown in Figure 6, are characterised by definite projection of the total angular moment of the anisotropy axis. In the Dy4 site, the ground and the first excited state anisotropic axes are in opposite directions, while in other three sites they are co-parallel.

To probe the mechanism of single-ion relaxation, data beyond the ground state KDs need to be analysed. The magnetic relaxation in lanthanides is found to occur due to three main factors, in the absence of intermolecular interactions,[10e] (i) *via* QTM between the

ground state KDs which occurs due to large transverse anisotropy in the ground state KDs, (ii) *via* Orbach/Raman processes[27] which accounts for the relaxation *via* the excited states and occurs due to the non-coincidence of the principle anisotropic axes, (iii) *via* thermally assisted QTM (TA-QTM) which accounts for relaxation *via* the excited states due to the non-Ising nature of the excited KDs. A qualitative mechanism of the relaxation for **1** obtained from *ab initio* calculations is shown in Figure 6. Here the states are arranged according to the values of their magnetic moments. The number at each arrow connecting any two states is the mean absolute value of the matrix elements of the transition magnetic moments between the corresponding states. For all the Dy sites (Dy1, Dy2, Dy3 and Dy4) the transverse anisotropy observed is small, and the QTM between the ground state KDs is expected to be weak.

Table 2. Calculated energy spectrum, *g*-tensors and tilt angles (θ) of the principal anisotropy axes of first excited state (ES) on Dy1, Dy2, Dy3 and Dy4 with respect to the ground state (GS) for complex **1**.

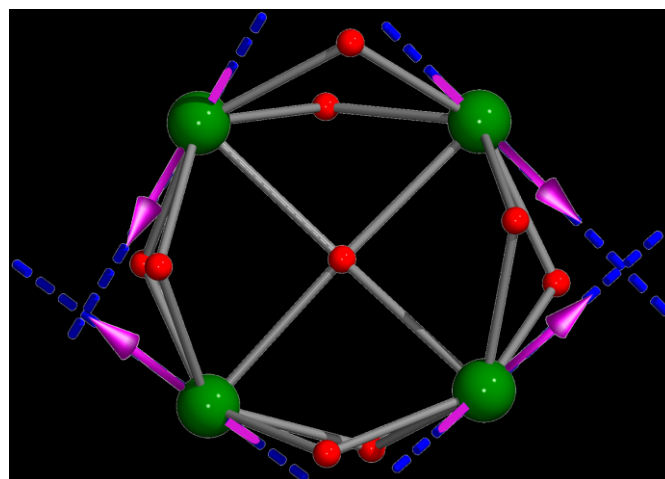| Sites		g_{xx}	g_{yy}	g_{zz}	energy (cm^{-1})	θ (°)
Dy1	GS KD	0.049	0.103	19.794	0.00	-
	1st ES KD	0.976	1.982	15.819	134.6	14.6
Dy2	GS KD	0.043	0.069	19.768	0.00	-
	1st ES KD	1.192	3.127	14.998	147.8	10.5
Dy3	GS KD	0.091	0.199	19.554	0.00	-
	1st ES KD	1.799	5.654	12.629	145.0	5.5
Dy4	GS KD	0.09	0.023	19.868	0.00	-
	1st ES KD	0.168	0.253	16.968	190.0	168.9

Fig.5. *Ab initio* computed ground Kramers Doublet state anisotropy axis along z-direction in **1**. The arrows exhibit coupled state orientation (ferromagnetic interaction between neighbours) Colour code: Dy(III): Green, O : red, N, C and H atoms have been removed for clarity.

Our calculations confirm this point, as shown in Figure 6a, where for both Dy1 and Dy4 centres the QTM between the ground state KDs is negligible. The next excited states (ES) are located at 135 cm^{-1}, 148 cm^{-1} and 145 cm^{-1} for Dy1, Dy2 and Dy3 centres, respectively, and these states possess significant transverse anisotropy. The g_{zz} axis deviates from the direction of the ground state KD by 14.6, 10.47 and 5.47° for Dy1, Dy2 and Dy3 centres, respectively (tilt angle, θ).

This naturally activates the Orbach/Raman type relaxation *via* the first excited state and, as expected, a significant magnetic moment matrix element is observed for this process Figure 6a. As the transverse anisotropy of the first excited state is large, this leads to a significant TA-QTM process, and this is also reflected in the computed parameters. The calculations find that ground and first excited state are predominantly |+-15/2>: 0.99 |+-15/2> and |+-13/2>: 0.91 |+-13/2>, respectively, for the Dy1, Dy2 and Dy3 sites. The Dy4 site on the other hand is distinctly different from other three sites in complex **1**, where the transverse anisotropy is not prominent in the ground state or first excited state. However as the tilt angle is large, this leads to relaxation *via* the first excited state. Thus for Dy4, the computed effective energy barrier (U_{cal}) is 190.0 cm^{-1} which is marginally higher than other sites. Thus, for the uncoupled Dy(III) sites, two relaxation processes are theoretically expected to operate, one at an average U_{cal} of 144 cm^{-1} (Dy1, Dy2 and Dy3) and other at 190 cm^{-1} (Dy4). In accordance with the theoretical prediction, there are two relaxations processes that are experimentally observed at 20.15 cm^{-1} and 69.5 cm^{-1} (29 and 100 K respectively, Figure 4). Hence, we can tentatively assign the faster relaxation process which occurs at lower temperature to the Dy1, Dy2 and Dy3 sites, and the slower magnetization relaxation process which occurs at higher temperature to Dy4. The large deviation in U_{eff} values between the calculated and experimental results can be attributed to the fact that the ground state QTM and the dipolar/exchange interactions (intra and inter) are not taken in to account in the estimate of the computed barriers. These issues have been discussed in detail in a previous experimental and theoretical study of Er(III) SMMs.[28] The argument of magnetization relaxation based on single-ion anisotropy is valid since the estimate of the exchange coupling between Dy(III) ions is extremely small (*vide infra*).

To offer a rationale on the differences observed between the four Dy sites, we have examined at the structural distortion (using SHAPE software)[21] at the individual Dy sites. The deviations are found to be 1.18, 1.22, 1.20 and 1.08 for Dy1, Dy2, Dy3 and Dy4 sites respectively (see Figure S9 in ESI), compared to an ideal mono-capped square anti-prismatic geometry. These numbers represent the extent of deviation from the ideal mono-capped square anti-prismatic geometry. Thus the larger distortion of Dy1, Dy2 and Dy3 compared to Dy4 leads to concomitant smaller barrier heights. To gain more insight into the mechanism of magnetization relaxation, we have also computed the crystal field parameters. Assuming that intermolecular and hyperfine interactions are small or negligible, the probability of QTM between the ground state KDs is best described by the crystal field (CF) parameters.[10h,29] The corresponding crystal field Hamiltonian is given by $H_{CF} = B_k^q O_k^q$, where B_k^q is the crystal field parameter, and O_k^q is the Steven's operator. QTM effects are expected to be dominant in a system where the non-axial B_k^q (where q ≠ 0, and k = 2, 4, 6) terms are larger than the axial B_k^q (where q = 0, and k = 2, 4, 6) terms (Table S6). The observation of small transverse anisotropy for all the Dy sites in **1** is also well reproduced in the computed CF parameters, where the non-axial B_2^1, B_2^2, B_4^{-3} and B_6^5 terms are larger than the axial terms (B_2^0, B_4^0, B_6^0) (Table

S6). We have also employed an electrostatic model to gain information regarding the orientation of the anisotropy axis of the ground state in complex **1**.[30] This axis is calculated to be close to the ground state *ab initio* anisotropic axis, with the deviation being approximately 12.91⁰, 9.28⁰, 14.09⁰ and 12.45⁰ for Dy1, Dy2, Dy3 and Dy4, respectively (Figure S9) suggesting that the orientation of the anisotropy axis is controlled predominantly by the electrostatic charges of the ligands.
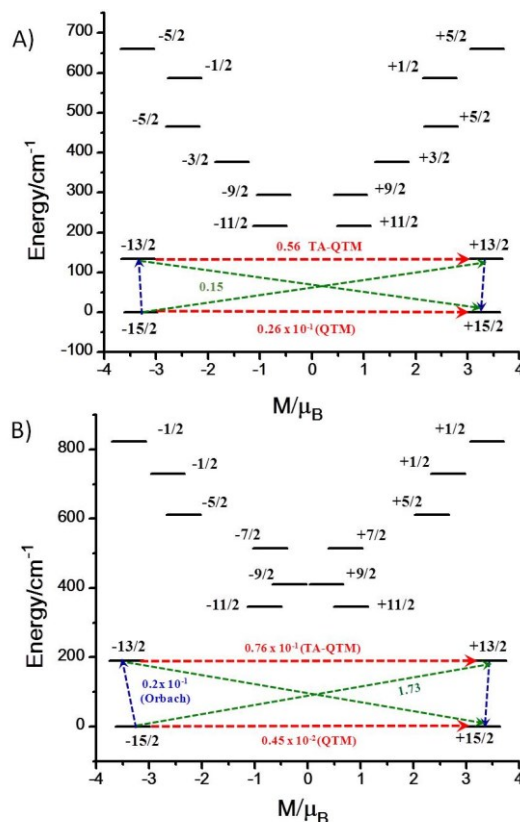

Fig 6. The *ab initio* computed magnetization blocking barrier for a) the Dy1 site (a similar picture is found for Dy2 and Dy3), b) the Dy4 site. The thick black line indicates the Kramers doublets (KDs) as a function of magnetic moment. The dotted green lines show the possible pathway of the Orbach process. The dotted blue lines show the most probable relaxation pathways for magnetization reversal. The dotted red lines represent the presence of QTM/TA-QTM between the connecting pairs. The numbers provided at each arrow are the mean absolute value for the corresponding matrix element of transition magnetic moment.

Exchange coupled {Dy₄} molecule: Due to the axiality of the Dy sites, we have simulated the magnetic interactions between Dy ions by incorporating contributions from magnetic dipole-dipole and exchange interactions within an Ising exchange Hamiltonian. We have also calculated the exchange spectrum (Figure 7) of complex **1** using the POLY_ANISO program. An excellent agreement between the simulated and experimental magnetic data ($\chi_M T$ (*T*) and *M* (*H*)) was observed with the parameters J_1 = +0.01 cm^{-1} and J_2 = -0.01 cm^{-1} (Figure 8). This is further corroborated by specific heat measurements that show a well-defined Schottky anomaly at liquid helium temperatures (*vide infra*). Our computed *g*-tensor for the exchange coupled system shows zero transverse anisotropy contribution, it is completely Ising in nature. Most importantly, the principal *g*-tensor (magnetic moment, Table S7) anisotropy of the

lowest (ground) exchange level of the exchange spectrum is 3.96. This observation of a conventional magnetic moment (a deviation from zero) in the ground state can be ascribed to the low-symmetry nature of the complex.
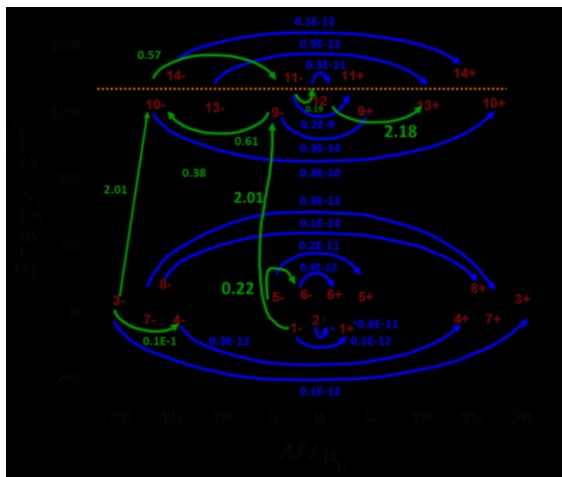

Fig 7. The low-lying exchange spectrum and magnetization blocking barrier in complex **1.** We have placed every exchange state in compliance with the value of its magnetic moment (bold black lines).The blue curved arrows signify tunneling of magnetization within each doublet state, green curved arrows represent spin-phonon transitions (the numbers are averaged transition moments in μ_B connecting the corresponding states).[31]

The first excited doublet of the exchange spectrum lies at a larger energy separation (4.4 cm^{-1}) with respect to the ground state, compared to a previously studied Dy$_4$ complex[32] (2.97 cm^{-1}) which introduces a very small low field S shape to the magnetization curve (Figure 8B inset) in complex **1.** This intramolecular coupling may facilitate preferential information storage compared to conventional SMMs.[7b] An analysis of the exchange spectrum of **1** (Table S7) clearly reveals a small magnetic moment matrix element for the ground-state exchange doublet (non-Kramers system) which subsequently suppresses the QTM completely (Figure 7, Table S7). These values for all other low-lying states (including excited states) are found to have low magnitudes, resulting in complete suppression of TA-QTM contributions to the magnetic relaxation. These observations lead to the occurrence of relaxation *via* a spin-phonon tunnelling mechanism through the excited states, as indicated by the green arrows in Figure 7.

Significant matrix elements computed between ±5 and ±6 (0.22) describes a barrier of reversal of magnetization of approximately 4.6 cm^{-1} (Figure 7, Table S7). Another important spin-phonon transition has been observed from the ground-state -1 component to the -9 excited state components, followed by transition from -9 to -10, -10 to -11, -11 to -12, -12 to -13 and eventually to the time-reversed states in the opposite order (green arrows in Figure 7). This is the sole pathway with concomitant substantial magnetic matrix elements connecting the ground state -1 with other excited states. Additionally, direct tunnelling transitions between higher excited states (*i.e.* between -9 and +9, -10 and -10) are less efficient due to the extremely small value of magnetic moment matrix elements being of the order of 10^{-10} μ_B. Hence, another barrier height can be envisioned occurring at approximately 138 cm^{-1} (as shown by the dotted orange line in Figure 7), which is similar to the slower

magnetization relaxation observed from the ac susceptibility measurements. The observation of such a multi-level-exchange spectrum corroborates the presence of a slow magnetization relaxation time in complex **1** due to the significantly quenched QTM and TA-QTM processes.
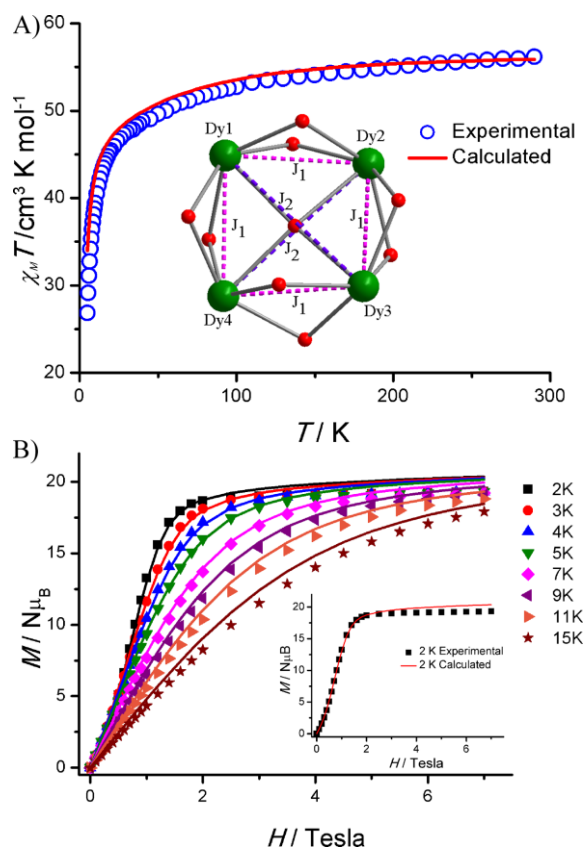

Fig 8. Poly_ANISO simulated (solid lines) (A) magnetic susceptibility and (B) magnetization data with respect to experimental (scattered symbol) in complex **1**. It is notable that intermolecular interaction zJ' was kept fixed at -0.14 cm^{-1}

The calculated *ab initio* and electrostatic anisotropy axes lie at a position which faces the least repulsion from the negatively charged μ_4-hydroxo ligand. Although not all four g_{zz} axes create a circular pattern, the projected magnetic moment due to g_{zz} being in the plane of the four lanthanide ion leads to a toroidal magnetic moment.[7b,33] This is rather clearly visible in the magnetization data measured at *T* = 2 K. This is similar to the toroidal moment observed in other Dy structures, such as the Dy$_6$ wheel, Dy$_3$ triangles, and Dy$_4$ butterfly complexes.[8,32-33] Analysis of the structural details of complex **1** indicates that it possesses a *pseudo* C$_4$ axis of symmetry. The g_{zz} axis of Dy1, Dy2 and Dy3 are in plane with respect to the pseudo C$_4$ axis, with tilts of 6.2°, 15.9° and 13.2° for Dy1, Dy2 and Dy3, respectively (Figure 5) and the deviations are within ~10 degrees. The Dy4 ion on the other hand deviates significantly from the pseudo C$_4$ axis with a tilt angle of 41.5°. However, the projected magnetic moment of all four Dy sites is expected to be on the square plane of the molecule leading to a toroidal moment. Although analogous square based complexes have been reported in the literature,[22,23] this is the first example where such a complex has

been shown, by *ab initio* calculations, to possess a toroidal magnetic moment.

***Single Ion Anisotropy of Tb(III) in complx 2*:** Complex **2** has ideal Ising type anisotropy, computed for all 13 states in all four Tb(III) ions (Tables S8-S11) which is also well reproduced by computed crystal field parameters (Table S12). For Tb1, Tb2, Tb3 and Tb4 five pseudo-doublets and three singlets were obtained (Table 3).

Table 3. Calculated energy spectrum, *g*-tensors and angles (°) of the principal anisotropy axes of the first excited states on Tb1, Tb2, Tb3 and Tb4 with respect to the ground state for complex **2**

	Level	Energy(cm⁻¹)	gz	angle(°)
Tb1 site	1	0.0	17.64	-
	2	0.13		
	3	98.77	14.45	9.41
	4	100.01		
Tb2 site	1	0.0	17.73	-
	2	0.095		
	3	111.92	14.37	49.03
	4	112.34		
Tb3 site	1	0.0	17.80	-
	2	0.06		
	3	128.64	14.50	173.03
	4	129.58		
Tb4 site	1	0.0	17.46	-
	2	0.18		
	3	142.96	13.85	5.23
	4	145.61		

Here, as in complex **1**, mirror symmetry of the magnetic energy levels is observed, *i.e.* a decrease of g_{zz} up to energy level four or five after which an increase is observed. This implies the presence of a low-symmetry environment around the Tb(III) centres (see Figure 9 and ESI S8 for the fragmented structure considered for calculation). The ground state is computed to be doubly degenerate with another state lying very close (0.1 cm⁻¹).
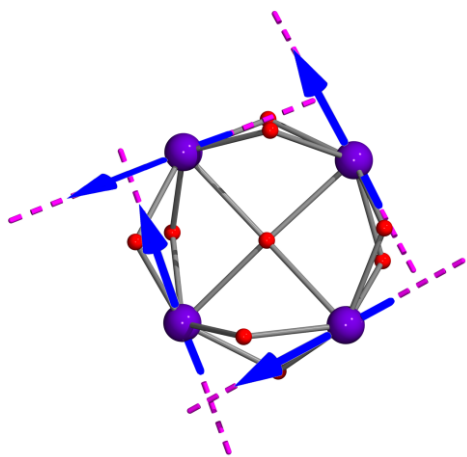

Fig 9. *Ab inito* computed ground state anisotropy axis along z direction in complex **2** for all the individual Tb[III] ions separately.(colour scheme: Tb[III]: Violet O : red, N : blue, C :grey and hydrogen atoms have been removed for clarity){Arrow colour scheme: Orange indicates g_z orientation of ground pseudo-doublet whereas blue denotes first excited pseudo-doublet}

The computed principal g-tensor anisotropy of the ground pseudo doublet in all the four Tb sites in **2** is found to possess large g_{zz} value (17.46-17.80). This value is close to the expected pure Ising g_{zz} value (18.0) expected for a mj = ±6 and this large g_{zz} magnitude is

also reflected for the highest energy pseudo-doublet. Substantial intrinsic tunnel splitting (i..e >10⁻⁴ cm⁻¹) in all the Tb sites of complex **2** induces major tunneling via the ground state which subsequently quenches the relaxation probability via the higher excited states deterring **2** to exhibit any SMM characteristics which is in line with the experimental ac measurements.[1b, 34]

Exchange coupled {Tb₄} molecule: Adapting same strategy employed in complex **1** for fitting the magnetic data, we have performed simulation for complex **2** using POLY_ANISO program (see Figure 10). Our simulation able to reproduce the magnetic data [$\chi_M T$ (T)] which consequences the observation of exchange parameters as +0.11 and -0.01 cm⁻¹ as J_1 and J_2 respectively (Figure 11 and Figure S10). Exchange coupled anisotropy for complex **2** is evidenced by complete Ising nature (Table S13) with zero transversal contribution. As per the SINGLE_ANISO analysis significant tunnel splitting (Δ_{tun}= 10⁻¹ cm⁻¹) in the ground doublet facilitate tunnelling and preclude any SMM characteristics in complex **2**.
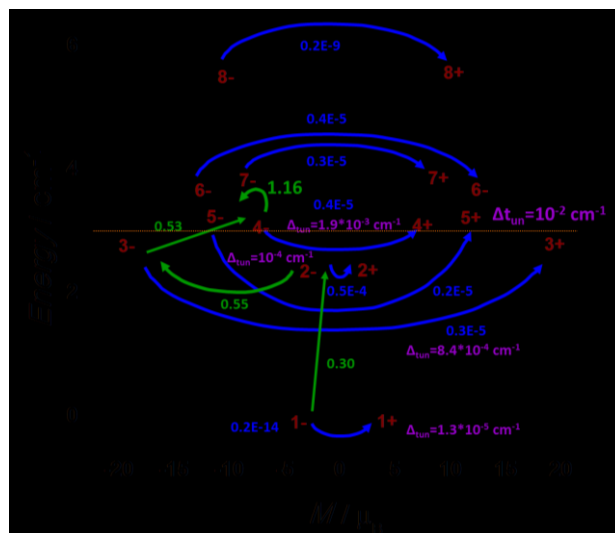

Fig 10. The low-lying exchange spectrum in complex **2**. We have placed every exchange state in compliance with the value of its magnetic moment (bold black lines).The blue curved arrows signify tunneling transitions within each doublet state (Δ_{tun}=corresponding tunnel gaps), green curved arrows represent spin-phonon transitions (the numbers are averaged transition moments in μ_B connecting the corresponding states)

Negligible magnetic moment matrix element (blue text and blue arrow in Figure 10) in the form of quantum tunnelling of magnetization (i.e. 10⁻¹⁴ μ_B) within the ground state doublets pushes up the relaxation further towards higher excited state. This is also corroborated by the non-significant (i..e Δ_{tun} <10⁻⁴ cm⁻¹: purple text in Figure 10) intrinsic tunnel splitting within the ground doublets owing to the non-Kramers nature of the Tb(III) ions. Siginificant tunneling transition has been detected within ±5 (10⁻² cm⁻¹) and ±4 (10⁻³ cm⁻¹) states and these relaxations thus corresponds to TA-QTM process. Also the Orbach/Raman process are computed to be efficient between these levels (see green text and green arrows in Figure 10), revealing the likelihood of complete relaxation of magnetization at this level which lies 3.3 cm⁻¹ away from the ground

state. Significantly low energy gap between the ground and first exited state rationalizes why complex **2** relaxes faster than **1** which is consistent with the experimental (small raise in χ_M'' at low temperature and high frequency limit) observations.
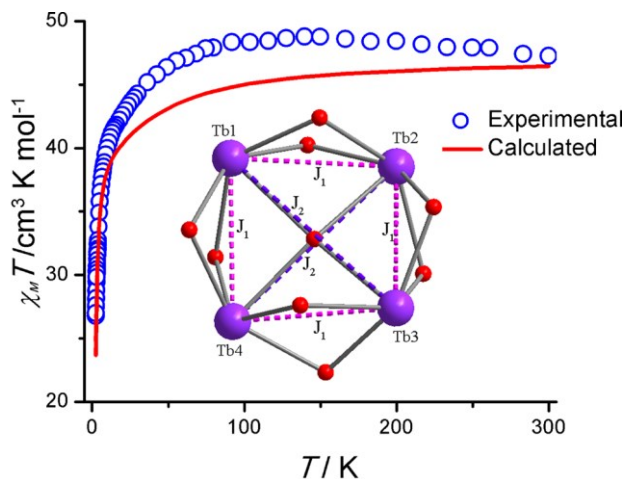

Fig 11. Poly_ANISO simulated (solid lines) magnetic susceptibility with respect to experimental (symbol) in complex **2**.

Estimation of Magnetocaloric Effect (MCE):

In order to evaluate the MCE efficiency of all the three complexes (**1-3**) detailed magnetization measurements (ESI Figures S2-S4) and field dependent heat capacity (Figure 12) measurements were performed on bulk samples. The change in magnetic entropy (-ΔS) and change in temperature (ΔT_{ad}) of the molecular cluster are the two essential thermodynamic parameters of MCE which can be precisely extracted from magnetization measurements using Maxwell's thermodynamic relation:

$$\Delta S_m(T,H) = \int_{H_i}^{H_f} \left[\frac{\partial M(T,H)}{\partial T} \right]_H dH$$

where H_i and H_f are the initial and final applied magnetic field, respectively. Complex **3** shows the maximum change in entropy (-$\Delta S_m = 23$ J Kg^{-1} K^{-1}) compared to **1** and **2**. The zero field splitting due to large spin-orbit coupling associated with **1** and **2** results in significantly lower degeneracy of the ground state. This leads to a smaller change in magnetic entropy value compared to a more isotropic clusters. Such scenario has been witnessed already in other lanthanide metal complexes reported elsewhere.[14h, 35]

To evaluate and validate the -ΔS_m extracted from magnetization measurements for **1-3**, heat capacity measurements were performed on polycrystalline samples at various temperature ranges (Figure 12). A large field independent contribution is observed above *ca.* 5K which is attributed to the lattice. This lattice contribution can be modelled by using an effective Debye model[36] $C_{latt}= A\ T^\alpha$, with α = 2.4 (for **1**, **2** and **3**) and A = 0.0095±10% (for **1**), A = 0.011±10% (for **2**), A = 0.010±10% (for **3**). This contribution is comparable for the three molecules, as expected from the near-identical structures.
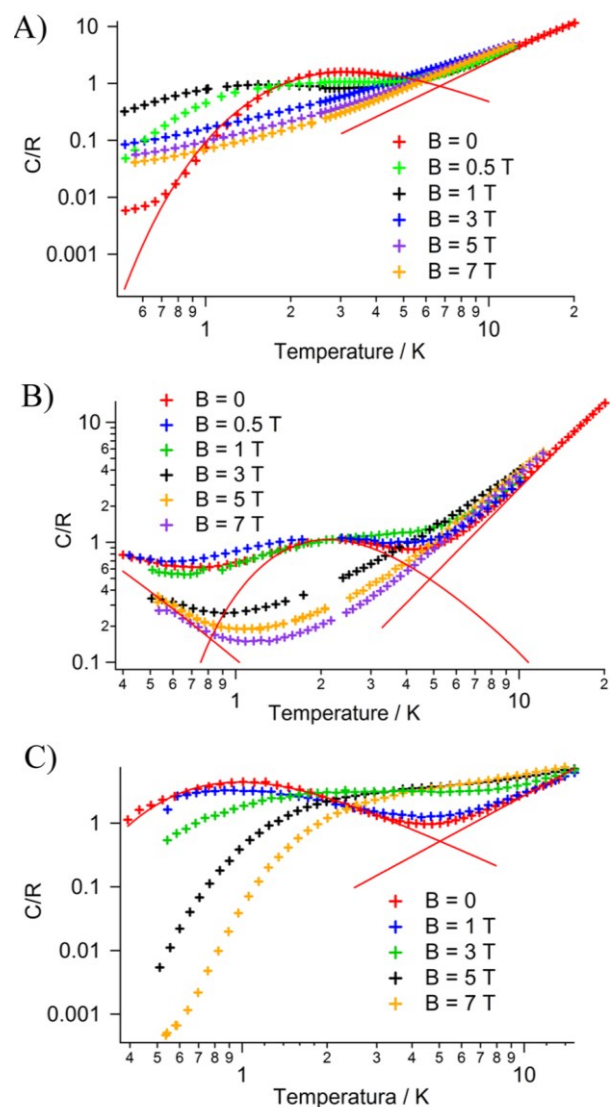

Fig 12. A-C) Temperature dependence of the heat capacity measured on polycrystalline samples of **1-3** at the indicated magnetic field (data normalized to gas constant R), Markers indicate the experimental data, while lines are the calculations described in the text.

A Schottky anomaly is evident in the low temperature specific heat of all three derivatives with a maximum at 1-2 K, arising from the magnetic exchange interactions between the magnetic ions. To get a rough idea of the strength of interaction we modelled this Schottky anomaly considering an effective split between two equally degenerate states separated by an energy gap T_0.

$$C_{int}/R = B\ (T_0/T)^2\ e^{(T_0/T)}/(1+e^{(T_0/T)})^2$$

Data fitting on the three $C(T)$ curves provides these values for the parameters B = 3.7 and T_0 = 7.78 K for **1**, B = 2.45 and T_0 = 5.1 K for **2**, B = 10 and T_0 = 2.35 K for **3**. In a first approximation the mean value of the exchange interactions J between four lanthanides leads to an effective gap $T_0 = 6\ J^2\ g_J^2\ J_{SE}$. In this way we are considering six equivalent interactions between the four magnetic ions, so what is found here is a mean value for J_{SE}. We found for **1**

J_{SE} = 0.0131K, for **2** J_{SE} = 0.0105K and for **3** J_{SE} = 0.0080K, comparable to J_1 and J_2 values theoretically estimated above. For **2**, another term is required to describe the upturn of the specific heat below 0.7K: the hyperfine coupling can be modelled using the hyperfine energy levels of terbium (0.120 K, 0.149 K and 0.178 K as respective gaps between the four hyperfine sublevels of the $J = 6$ multiplet and a multi-level Schottky anomaly expression.

The magnetic entropy (S_m) also can be evaluated from $S_m(T, H) = \int C_m/T \, dT$ where C_m is magnetic heat capacity directly obtained from heat capacity measurements. Notably, the extracted values are consistent with the values obtained from magnetization measurements. As expected, complex **3**, shows the largest $-\Delta S_m$ among the three complexes (Figure 13). The maximum value obtained for a 7T – 0 demagnetization is $-\Delta S_m$=(5.8 ± 0.6)R = 23 J Kg^{-1} K^{-1} at $T \simeq$ 3K for **3**; $-\Delta S_m$=(2.2 ± 0.4)R at $T \simeq$ 6K for **1** and $-\Delta S_m$=(2.0 ± 0.4)R at $T \simeq$ 5K for **2** (Figures S11-S12).

The observed $-\Delta S_m$ value for **3** is one of the largest known for an isotropic complexes, however this is significantly lower than the other isotropic metal complexes reported in the literature.[14e, 14h, 16, 37] Interestingly the $-\Delta S_m$ value expressed in J kg^{-1} K^{-1} units for **3** is larger than what reported for Gd$_4$Zn$_8$[14c] which contain similar squared Gd$_4$ core: this is in part due to the lighter mass of our **3** derivative, confirming the strategy of using lighter compound to enhance MCE.
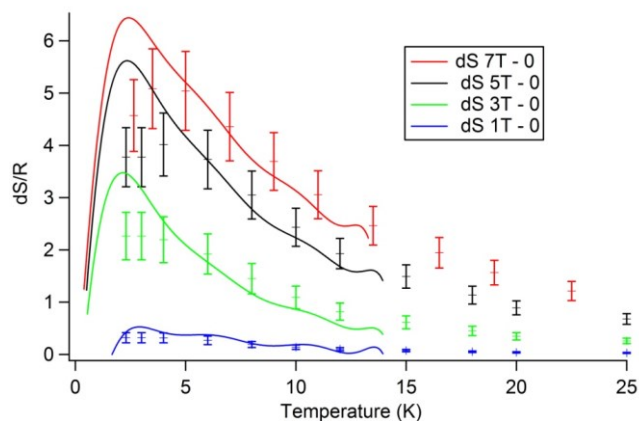

Fig 13. Entropy variation estimated from both magnetization measurements (points) and specific (lines) heat measurements for **1** for different magnetic field changes.

For an uncoupled four Gd(III) ions, the theoretically expected $-\Delta S_m$ value is 20.8 J kg^{-1} K^{-1}, however experimentally we observe more than the uncoupled value signifying that the excited states also participate in polarizing the spins. Accessibility of these excited states possible in case of **3** even at low temperature is likely due to the weak exchange interactions.

Experimental

All reagents and solvents were purchased from commercially available sources (Alfa Aesar and Sigma-Aldrich) and were used without further purification. All reactions were carried out under aerobic conditions unless otherwise stated. The ligand H$_4$L was synthesized as per the literature report,[18d] with a slight modification to improve the yield of the reaction; see below for details.

The chosen crystal was mounted on a Goniometer using paraffin oil and the crystal cooled in stream of liquid nitrogen to 100 K (for **1** and **3**), for **2** data were collected at room temperature. The data collection was done on a Rigaku Saturn CCD diffractometer (for **1** and **3**) and an Oxford CCD diffractometer for **2** using a graphite monochromator (λ = 0.71073º) equipped with an Oxford cryosystems cooler device. The unit cell determination and data reduction were performed using Rigaku CrystalClear-SM Expert 2.1 software. The structures were solved by direct methods and the refined by least-squares procedures on F^2 with SHELXTL package. All non-hydrogen atoms were refined anisotropically. Hydrogen atoms were placed based on the geometry and refined with a riding model. The solvents molecules were heavily disordered which we could not model it due to diffused electron density for all the three complexes. We have used the SQUZEE routine from PLATON resulted in smooth refinement of the structures. The loop corresponds to residual electron density void (from PLATON) found in the structure is appended in its corresponding CIF files.

NMR spectra were recorded for the H$_4$L ligand on a Bruker Avance III 400 MHz instrument at room temperature. The data were calibrated with listed deuterated solvents. Infrared spectra were collected for the solid samples using KBr pellets on a Perkin-Elmer FT-IR spectrometer in the 400 to 4000 cm^{-1} range. Variable temperature dc susceptibility measurements were performed on a Quantum Design MPMS-SQUID Magnetometer. Diamagnetic corrections were applied for the constituent atoms using Pascal's constants. Heat capacity measurements were measured on a PPMS-7T system using the two tau method. Microcrystals were pressed into thin pellets and cut in thin slices of 1-2 mg in weight.

Synthesis of H$_4$L

In a 250 mL RB flask a methanolic solution of *o*-vanillin (5.0002 g, 0.0328 mol, 100 mL MeOH) was added 5-6 drops of glacial acetic acid (0.3 mL) added drop by drop in order to activate the carbonyl group in *o*-vanillin and stirred for 10 minutes. Into the reaction flask, solid tris(hydroxymethyl)aminomethane (3.981 g, 0.0328 mol) was then added and the reaction mixture heated under reflux for 24 hours. The light yellow precipitate formed was filtered and washed with *n*-hexane several times and dried under vacuum. The purity of the ligand was confirmed by ^{1}H NMR and ^{13}C NMR recorded in DMSO-d$_6$. ^{1}H NMR (400 MHz): δ (ppm) 14.7(s, 1H), 8.48(s, 1H), 6.92(dd, J=7.88 Hz, 2H), 6.57(t, J=7.84 Hz, 1H), 4.84(s, 3H), 3.73(s, 3H), 3.6 (d, 6H). ^{13}C NMRδ (ppm): 164.11(C=N), 158.17, 149.53, 124.15, 117.12, 114.86, 114.33, 66.43, 61.11, 55.72. FT-IR (KBr

pellet, cm^{-1}): 2919 cm^{-1} (s, $\nu_{(Ar-H)}$), 1644 cm^{-1} (s, $\nu_{(C=N)}$). Yield =7.56 g, 90%).

Synthesis of complex 1:

A methanolic solution (30 mL) of H$_4$L (0.300 g, 1.175 mmol) was deprotonated by using NaOMe (0.1269 g, 2.350 mmol) and the solution stirred for 30 minutes before charging DyCl$_3$·xH$_2$O (0.3159 g, 1.175 mmol) into the reaction flask. The resultant reaction mixture was stirred for 24 hours and then filtered. The filtrate volume was reduced to one-third of its initial volume and kept for crystallization without any disturbance. Pale yellow block-shaped single crystals were grown from the filtrate after one week, and were suitable for X-ray diffraction. Yield: 142 mg, (27%, based on Dy). Elemental analysis (air dried sample) (%): Calculated: C, 29.8; H, 4.9; N, 2.7; Found: C, 30.1; H, 4.6; N, 2.6; FT-IR (KBr pellet, cm^{-1}): 2921 cm^{-1} (s, $\nu_{(Ar-H)}$), 1648 cm^{-1} (s, $\nu_{(C=N)}$).

Synthesis of complexes 2 and 3:

The same procedure was followed for complex **1,** but using the corresponding equivalence of lanthanide halides (TbCl$_3$·6H$_2$O (0.4388 g, 1.175 mmol for **2** and GdBr$_3$·xH$_2$O (0.4665 g, 1.175 mmol) for **3**) in place DyCl$_3$.xH$_2$O. For **2**: Yield: 137mg, (25%, based on the Tb). Elemental analysis (air dried sample) (%): Calculated: C, 32.6; H, 4.7; N, 2.7; Found: C, 32.1; H, 4.8; N, 2.6; FT-IR (KBr pellet, cm^{-1}): 2924 cm^{-1} (s, $\nu_{(Ar-H)}$), 1644 cm^{-1} (s, $\nu_{(C=N)}$). For **3**: Yield: 145 mg, (26%, based on the Gd). Elemental analysis (dried sample) (%): Calculated: C, 31.6; H, 4.6; N, 2.6; Found: C, 31.2; H, 4.7; N, 2.6; FT-IR (KBr pellet, cm^{-1}): 2926 cm^{-1} (s, $\nu_{(Ar-H)}$), 1646 cm^{-1} (s, $\nu_{(C=N)}$).

Conclusions

In this article we have reported an unusual family of O-centred Ln$_4$ (where Ln = Dy, Tb or Gd) squares whose structures were determined by single crystal X-ray diffraction. DC magnetic susceptibility data on complexes **1-3** show the presence of weak antiferromagnetic interactions between the metal ions. Unambiguous evidence for the existence of antiferromagnetic interaction between the anisotropic lanthanide ions is confirmed through *ab initio* calculations and heat capacity measurements. Ac susceptibility measurements performed on anisotropic complexes **1** and **2** in the 2.0 - 35 K temperature range reveal both complexes to show frequency dependent out-of-phase signals (χ_M''), although the maxima in χ_M'' for **2** is below the instrument temperature limit. On the other hand, complex **1** shows two different magnetization relaxation processes, one at high temperature and one at low temperature. The Arrhenius plot constructed from these two relaxation processes reveals the barrier height for magnetization vector reversal of 29 K and 100 K. We have rationalized the origin of these two relaxations processes in complex **1** by detailed *ab initio* calculations, which demonstrated that the Dy4 site in complex **1** behaves differently compared to the other three sites. Calculations reveal the existence of a toroidal magnetic moment complex **1**, with experimental evidence confirmed from the *S*-shaped

magnetization curve measured at 2.0 K. The exchange interaction extracted using the POLY_ANISO program is in agreement with experimentally derived parameters. The MCE of all the three complexes were estimated from two different experimental techniques, field dependent magnetization and heat capacity measurements, with complex **3** showing the largest change in magnetic entropy (23 J Kg^{-1} K^{-1}), due to the near isotropic nature of the ground state and weak exchange interactions. The three analogous square based complexes are therefore a family of complexes exhibiting unusual physical properties, including toroidal magnetic moments, SMM behaviour and an enhanced MCE.

Acknowledgements

Notes and references

^{a}*Department of Chemistry, Indian Institute of Technology Bombay, Powai, Mumbai, Maharashtra, India-400076.*

^{b}*CNR, Institute of Nanosciences S3 and Dipartimento di Scienze Fisiche, Informatiche e Matematiche, Università di Modena e Reggio Emilia, via G. Campi213/A, 41125 Modena, Italy*

^{c}*EaStCHEM School of Chemistry, The University of Edinburgh, David Brewster Road, Edinburgh, EH9 3FJ, UK.*

Electronic Supplementary Information (ESI) available: The relevant magnetic, thermal data and computational details along with energy profiles for the computed energy levels are given in ESI. CCDC numbers: 1060622-1060624. See DOI: 10.1039/b000000x/

References:

1   a) G. Aromi and E. K. Brechin, *Struct. Bonding.* **2006**, *122*, 1-67; b) R. J. Blagg, L. Ungur, F. Tuna, J. Speak, P. Comar, D. Collison, W. Wernsdorfer, E. J. L. McInnes, L. F. Chibotaru and R. E. P. Winpenny, *Nat. Chem.* **2013**, *5*, 673-678; c) D. Gatteschi, A. Caneschi, L. Pardi and R. Sessoli, *Science.* **1994**, *265*, 1054-1058; d) M. Mannini, F. Pineider, C. Danieli, F. Totti, L. Sorace, P. Sainctavit, M. A. Arrio, E. Otero, L. Joly, J. C. Cezar, A. Cornia and R. Sessoli, *Nature.* **2010**, *468*, 417-421; e) M. Mannini, F. Pineider, P. Sainctavit, C. Danieli, E. Otero, C. Sciancalepore, A. M. Talarico, M.-A. Arrio, A. Cornia, D. Gatteschi and R. Sessoli, *Nat. Mater.* **2009**, *8*, 194-197; f) R. Sessoli, D. Gatteschi, A. Caneschi and M. A. Novak, *Nature.* **1993**, *365*, 141-143; g) R. Sessoli, H. L. Tsai, A. R. Schake, S. Wang, J. B. Vincent, K. Folting, D. Gatteschi, G. Christou and D. N. Hendrickson, *J. Am. Chem. Soc.* **1993**, *115*, 1804-1816; h) D. N. Woodruff, R. E. P. Winpenny and R. A. Layfield, *Chem. Rev.* **2013**, *113*, 5110-5148.

2   a) L. Bogani and W. Wernsdorfer, *Nat. Mater.* **2008**, *7*, 179-186; b) S. Sanvito and A. R. Rocha, *J. Comput. Theor. Nanosci.* **2006**, *3*, 624-642; c) W. Wernsdorfer, *Int. J. Nanotechnol.* **2010**, *7*, 497-522.

3   a) C. P. Collier, G. Matterstei, E. W. Wong, Y. Luo, K. Beverly, J. Sampaio, F. M. Raymo, J. F. Stoddart and J. R. Heath, *Science.* **2000**, *289*, 1172-1175; b) A. R. Pease, J. O. Jeppesen, J. F. Stoddart, Y. Luo, C. P. Collier and J. R. Heath, *Acc. Chem. Res.* **2001**, *34*, 433-444.

4   a) F. R. Renani and G. Kirczenow, *Phys. Rev. B Condens. Matter Mater. Phys.* **2013**, *87*, 121403/121401-121403/121405; b) M. Urdampilleta, S. Klyatskaya, J. P. Cleuziou, M. Ruben and W. Wernsdorfer, *Nat. Mater.* **2011**, *10*, 502-506.

5   D. Aguila, L. A. Barrios, V. Velasco, O. Roubeau, A. Repolles, P. J. Alonso, J. Sese, S. J. Teat, F. Luis and G. Aromi, *J. Am. Chem. Soc.* **2014**, *136*, 14215-14222.

6   N. Ishikawa, M. Sugita, T. Ishikawa, S.-Y. Koshihara and Y. Kaizu, *J. Am. Chem. Soc.* **2003**, *125*, 8694-8695.

7   a) H. L. C. Feltham and S. Brooker, *Coord. Chem. Rev.* **2014**, *276*, 1-33; b) L. Ungur, S.-Y. Lin, J. Tang and L. F. Chibotaru, *Chem. Soc. Rev.* **2014**, *43*, 6894-6905; c) R. A. Layfield, *Organometallics* **2014**, *33*, 1084-1099; d) L.-X. Chang, G. Xiong, L. Wang, P. Cheng and B. Zhao, *Chem. Commun.* **2013**, *49*, 1055-1057.

8   J. Tang, I. Hewitt, N. T. Madhu, G. Chastanet, W. Wernsdorfer, C. E. Anson, C. Benelli, R. Sessoli and A. K. Powell, *Angew. Chem., Int. Ed.* **2006**, *45*, 1729-1733.

9   J. D. Rinehart, M. Fang, W. J. Evans and J. R. Long, *J. Am. Chem. Soc.* **2011**, *133*, 14236-14239.

10. a) M. A. AlDamen, S. Cardona-Serra, J. M. Clemente-Juan, E. Coronado, A. Gaita-Arino, C. Marti-Gastaldo, F. Luis and O. Montero, *Inorg. Chem.* **2009**, *48*, 3467-3479; b) M. A. AlDamen, J. M. Clemente-Juan, E. Coronado, C. Marti-Gastaldo and A. Gaita-Arino, *J. Am. Chem. Soc.* **2008**, *130*, 8874-8875; c) S. Cardona-Serra, J. M. Clemente-Juan, E. Coronado, A. Gaita-Arino, A. Camon, M. Evangelisti, F. Luis, M. J. Martinez-Perez and J. Sese, *J. Am. Chem. Soc.* **2012**, *134*, 14982-14990; d) S. Ghosh, S. Datta, L. Friend, S. Cardona-Serra, A. Gaita-Arino, E. Coronado and S. Hill, *Dalton Trans.* **2012**, *41*, 13697-13704; e) N. Ishikawa, M. Sugita, T. Ishikawa, S. Koshihara and Y. Kaizu, *J. Phys. Chem. B* **2004**, *108*, 11265-11271; f) N. Ishikawa, M. Sugita, N. Tanaka, T. Ishikawa, S.-Y. Koshihara and Y. Kaizu, *Inorg. Chem.* **2004**, *43*, 5498-5500; g) J. Kan, H. Wang, W. Sun, W. Cao, J. Tao and J. Jiang, *Inorg. Chem.* **2013**, *52*, 8505-8510; h) J. J. Le Roy, M. Jeletic, S. I. Gorelsky, I. Korobkov, L. Ungur, L. F. Chibotaru and M. Murugesu, *J. Am. Chem. Soc.* **2013**, *135*, 3502-3510; i) J. D. Rinehart and J. R. Long, *Chem. Sci.* **2011**, *2*, 2078-2085.

11   a) S. Aime, M. Botta and E. Terreno, *Adv. Inorg. Chem.* **2005**, *57*, 173-237; b) P. Caravan, *Chem. Soc. Rev.* **2006**, *35*, 512-523; c) A. Datta and K. N. Raymond, *Acc. Chem. Res.* **2009**, *42*, 938-947; d) P. Hermann, J. Kotek, V. Kubicek and I. Lukes, *Dalton Trans.* **2008**, 3027-3047; e) J. Lee, M. J. Zylka, D. J. Anderson, J. E. Burdette, T. K. Woodruff and T. J. Meade, *J. Am. Chem. Soc.* **2005**, *127*, 13164-13166; f) E. C. Wiener, M. W. Brechbiel, H. Brothers, R. L. Magin, O. A. Gansow, D. A. Tomalia and P. C. Lauterbur, *Magn. Reson. Med.* **1994**, *31*, 1-8; g) C.-T. Yang, P. Chandrasekharan, T. He, Z. Poh, A. Raju, K.-H. Chuang and E. G. Robins, *Biomaterials* **2014**, *35*, 327-336.

12   a) A. Martorana, G. Bellapadrona, A. Feintuch, E. Di Gregorio, S. Aime and D. Goldfarb, *J. Am. Chem. Soc.* **2014**, *136*, 13458-13465; b) A. M. Raitsimring, C. Gunanathan, A. Potapov, I. Efremenko, J. M. L. Martin, D. Milstein and D. Goldfarb, *J. Am. Chem. Soc.* **2007**, *129*, 14138-14139.

13   a) B. Corzilius, A. A. Smith, A. B. Barnes, C. Luchinat, I. Bertini and R. G. Griffin, *J. Am. Chem. Soc.* **2011**, *133*, 5648-5651; b) J. W. Gordon, S. B. Fain and I. J. Rowland, *Magn. Reson. Med.* **2012**, *68*, 1949-1954.

14   a) E. Colacio, J. Ruiz, G. Lorusso, E. K. Brechin and M. Evangelisti, *Chem. Commun.* **2013**, *49*, 3845-3847; b) I. A. Gass, E. K. Brechin and M. Evangelisti, *Polyhedron* **2013**, *52*, 1177-1180; c) T. N. Hooper, J. Schnack, S. Piligkos, M. Evangelisti and E. K. Brechin, *Angew. Chem., Int. Ed.* **2012**, *51*, 4633-4636, S4633/4631-S4633/4633; d) G. Lorusso, M. A. Palacios, G. S. Nichol, E. K. Brechin, O. Roubeau and M. Evangelisti, *Chem. Commun.* **2012**, *48*, 7592-7594; e) G. Lorusso, J. W. Sharples, E. Palacios, O. Roubeau, E. K. Brechin, R. Sessoli, A. Rossin, F. Tuna, E. J. L. McInnes, D. Collison and M. Evangelisti, *Adv. Mater.* **2013**, *25*, 4653-4656; f) V. K. Pecharsky and K. A. Gschneidner, Jr., *J. Magn. Magn. Mater.* **1999**, *200*, 44-56; g) A. M. Tishin, A. V. Derkach, Y. I. Spichkin, M. D. Kuz'min, A. S. Chernyshov, K. A. Gschneidner and V. K. Pecharsky, *J. Magn. Magn. Mater.* **2007**, *310*, 2800-2804; h) Y.-Z. Zheng, M. Evangelisti, F. Tuna and R. E. P. Winpenny, *J. Am. Chem. Soc.* **2012**, *134*, 1057-1065.

15   R. D. McMichael, R. D. Shull, L. J. Swartzendruber, L. H. Bennett and R. E. Watson, *J. Magn. Magn. Mater.* **1992**, *111*, 29-33.

16   M. Evangelisti, O. Roubeau, E. Palacios, A. Camon, T. N. Hooper, E. K. Brechin and J. J. Alonso, *Angew. Chem., Int. Ed.* **2011**, *50*, 6606-6609, S6606/6601-S6606/6605.

17   a) G. Asgedom, A. Sreedhara, J. Kivikoski, J. Valkonen, E. Kolehmainen and C. P. Rao, *Inorg. Chem.* **1996**, *35*, 5674-5683; b) D. F. Back, C. R. Kopp, G. Manzoni de Oliveira and P. C. Piquini, *Polyhedron* **2012**, *36*, 21-29; c) V. Chandrasekhar, A. Dey, A. J. Mota and E. Colacio, *Inorg. Chem.* **2013**, *52*, 4554-4561; d) D. Liu, Q. Zhou, Y. Chen, F. Yang, Y. Yu, Z. Shi and S. Feng, *Dalton Trans.* **2010**, *39*, 5504-5508; e) C. P. Rao, A. Sreedhara, P. V. Rao, M. B. Verghese, K. Rissanen, E. Kolehmainen, N. K. Lokanath, M. A. Sridhar and J. S. Prasad, *J. Chem. Soc., Dalton Trans.* **1998**, 2383-2394; f) Y. Sui, X. Zeng, X. Fang, X. Fu, Y. a. Xiao, L. Chen, M. Li and S. Cheng, *J. Mol. Catal. A Chem.* **2007**, *270*, 61-67; g) X. Zhang, P. Wei, J. Dou, B. Li and B. Hu, *Acta Crystallogr., Sect. E Struct. Rep. Online* **2009**, *65*, m293-m294, m293/291-m293/211.

18   a) H. Ke, L. Zhao, Y. Guo and J. Tang, *Dalton Trans.* **2012**, *41*, 9760-9765; b) H. Ke, L. Zhao, Y. Guo and J. Tang, *Dalton Trans.* **2012**, *41*, 2314-2319; c) H. S. Ke, Y. Guo, L. Zhao and J. K. Tang, *Sci. China Chem.* **2012**, *55*, 906-909; d) G. Wu, I. J. Hewitt, S. Mameri, Y. Lan, R. Clerac, C. E. Anson, S. Qiu and A. K. Powell, *Inorg. Chem.* **2007**, *46*, 7229-7231.

19   a) R. Bircher, B. F. Abrahams, H. U. Guedel and C. Boskovic, *Polyhedron* **2007**, *26*, 3023-3028; b) H. Ke, G.-F. Xu, L. Zhao, J. Tang, X.-Y. Zhang and H.-J. Zhang, *Chem. - Eur. J.* **2009**, *15*, 10335-10338; c) H. Ke, L. Zhao, G.-F. Xu, Y.-N. Guo, J. Tang, X.-Y. Zhang and H.-J. Zhang, *Dalton Trans.* **2009**, 10609-10613.

20   I. D. Brown and K. K. Wu, *Acta Crystallogr., Sect. B* **1976**, *B32*, 1957-1959.

21   a) H. Zabrodsky, S. Peleg and D. Avnir, *J. Am. Chem. Soc.* **1992**, *114*, 7843-7851; b) H. Zabrodsky, S. Peleg and D. Avnir, *J. Am. Chem. Soc.* **1993**, *115*, 8278-8289.

22   a) P.-H. Lin, I. Korobkov, W. Wernsdorfer, L. Ungur, L. F. Chibotaru and M. Murugesu, *Eur. J. Inorg. Chem.* **2011**, 1535-1539; b) N. M. Randell, M. U. Anwar, M. W. Drover, L. N. Dawe and L. K. Thompson, *Inorg. Chem.* **2013**, *52*, 6731-6742; c) A. Wai-Hing Lam, W.-T. Wong, G. Wen, X.-X. Zhang and S. Gao, *New J. Chem.* **2001**, *25*, 531-533.

23   M. U. Anwar, L. K. Thompson, L. N. Dawe, F. Habib and M. Murugesu, *Chem. Commun.* **2012**, *48*, 4576-4578.

24   N. F. Chilton, R. P. Anderson, L. D. Turner, A. Soncini and K. S. Murray, *J. Comput. Chem.* **2013**, *34*, 1164-1175.

25   D. N. Woodruff, F. Tuna, M. Bodensteiner, R. E. P. Winpenny and R. A. Layfield, *Organometallics* **2013**, *32*, 1224-1229.

26   a) J. M. Zadrozny, M. Atanasov, A. M. Bryan, C.-Y. Lin, B. D. Rekken, P. P. Power, F. Neese and J. R. Long, *Chem. Sci.* **2013**, *4*, 125-138; b) A. Arauzo, A. Lazarescu, S. Shova, E. Bartolome, R. Cases, J. Luzon, J. Bartolome and C. Turta, *Dalton Trans.* **2014**, *43*, 12342-12356; c) S. M. J. Aubin, Z. Sun, L. Pardi, J. Krzystek, K. Folting, L.-C. Brunel, A. L. Rheingold, G. Christou and D. N. Hendrickson, *Inorg. Chem.* **1999**, *38*, 5329-5340.

27   R. Orbach, *Proc. R. Soc. London, Ser. A* **1961**, *264*, 485-495.

28   a) S. K. Singh, T. Gupta, M. Shanmugam and G. Rajaraman, *Chem. Commun.* **2014**, *50*, 15513-15516; b) C. Das, A. Upadhyay, S. Vaidya, S. K. Singh, G. Rajaraman and M. Shanmugam, *Chem. Commun.* **2015**, *51*, 6173.

29   S. K. Langley, D. P. Wielechowski, V. Vieru, N. F. Chilton, B. Moubaraki, L. F. Chibotaru and K. S. Murray, *Chem. Sci.* **2014**, *5*, 3246-3256.

30   F. Chilton Nicholas, D. Collison, J. L. McInnes Eric, E. P. Winpenny Richard and A. Soncini, *Nat Commun.* **2013**, *4*, 2551.

31   S. K. Langley, D. P. Wielechowski, V. Vieru, N. F. Chilton, B. Moubaraki, B. F. Abrahams, L. F. Chibotaru and K. S. Murray, *Angew. Chem., Int. Ed.* **2013**, *52*, 12014-12019.

32   P.-H. Guo, J.-L. Liu, Z.-M. Zhang, L. Ungur, L. F. Chibotaru, J.-D. Leng, F.-S. Guo and M.-L. Tong, *Inorg. Chem.* **2012**, *51*, 1233-1235.

33   L. Ungur, S. K. Langley, T. N. Hooper, B. Moubaraki, E. K. Brechin, K. S. Murray and L. F. Chibotaru, *J. Am. Chem. Soc.* **2012**, *134*, 18554-18557.

34   a) L. Ungur, M. Thewissen, J.-P. Costes, W. Wernsdorfer and L. F. Chibotaru, *Inorg. Chem.* **2013**, *52*, 6328-6337; b) F.-S. Guo, J.-L. Liu, J.-D. Leng, Z.-S. Meng, Z.-J. Lin, M.-L. Tong, S. Gao, L. Ungur and L. F. Chibotaru, *Chem. - Eur. J.* **2011**, *17*, 2458-2466, S2458/2451-S2458/2452.

35   Y.-Z. Zheng, M. Evangelisti and R. E. P. Winpenny, *Angew. Chem., Int. Ed.* **2011**, *50*, 3692-3695, S3692/3691-S3692/3694.

36   M. Evangelisti, F. Luis, L. J. de Jongh and M. Affronte, *J. Mater. Chem.* **2006**, *16*, 2534-2549.

37   a) S. K. Langley, N. F. Chilton, B. Moubaraki, T. Hooper, E. K. Brechin, M. Evangelisti and K. S. Murray, *Chem. Sci.* **2011**, *2*, 1166-1169; b) J.-B. Peng, Q.-C. Zhang, X.-J. Kong, Y.-Z. Zheng, Y.-P. Ren, L.-S. Long, R.-B. Huang, L.-S. Zheng and Z. Zheng, *J. Am. Chem. Soc.* **2012**, *134*, 3314-3317.